Pure Appl. Chem., Vol. 81, No. 10, pp. 1931–1952, 2009.
doi:10.1351/PAC-CON-08-07-05
© 2009 IUPAC, Publication date (Web): 3 October 2009

Quasi-isothermal temperature-modulated differential scanning calorimetry (TMDSC) for the separation of reversible and irreversible thermodynamic changes in glass transition and melting ranges of flexible macromolecules*

Bernhard Wunderlich

Department of Chemistry, University of Tennessee, Knoxville, TN 37996, USA

Abstract: With standard differential scanning calorimetry (DSC), it is possible to derive calorimetric data for equilibrium or metastable samples. The introduction of temperature-modulated DSC (TMDSC) permits in its quasi-isothermal (non-scanning) mode (TMDC), long-time apparent heat capacity measurements of high precision (±1 %). For flexible molecules, heat capacity measurements from the various calorimetric methods could be combined in the ATHAS Data Bank, which now contains experimental data for over 200 materials. These data were linked to the vibrational and large-amplitude motion of the constituent atoms and molecules, to provide a base for the judgement of the thermal analyses, extending outside the range of equilibrium or metastability with an error of only 2–5 %. The TMDC together with DSC is now able to quantitatively assess the reversibility of thermal processes. A sufficient number of systems have been analyzed in this fashion to develop better understanding of macro-, micro-, and nanophases of flexible macromolecules. The new concepts discussed are: (1) multiple glass transitions due to possible rigid-amorphous fractions (RAFs) and glass transitions within crystals, both observed in semicrystalline macromolecules, and (2) locally reversible melting on the surface of chain-folded crystals. The locally reversible melting decreases with crystal perfection and also disappears when the chains become rigid.

Keywords: temperature-modulated DSC; glass transition; quasi-isothermal calorimetry; terminology; reversible melting/crystallization; melting transition.

HISTORICAL INTRODUCTION

Today, it is well known that *heat* is a form of energy exchanged between systems and has its microscopic origin in molecular motion [1]. By the 18th century, the term *caloric* was coined to describe what was thought to be the substance of heat. With this definition, heat could be measured quantitatively, irrespective of the missing understanding of the origin of heat [2]. The measurement of unknown heat effects always involves its comparison to a known effect. The most common unit to be matched in such measurements was the gram-calorie. It represented the amount of energy transferred to heat 1 g of water

*Paper based on a presentation at the 20th International Conference on Chemical Thermodynamics (ICCT 20), 3–8 August 2008, Warsaw, Poland. Other presentations are published in this issue, pp. 1719–1959.

by 1 °C at constant volume or pressure, the specific heat capacities c_v and c_p. At the beginning of the 20th century, the comparison to electrically produced heat became more precise and convenient, so that the calorie was abolished and replaced by the SI unit for energy and work, the joule (m^2 kg s^{-2}), measured in watt seconds.

Of the various calorimeters, the adiabatic calorimeter, differential scanning calorimeter (DSC), temperature-modulated differential scanning calorimeter (TMDSC), and quasi-isothermal, non-scanning version of TMDSC (TMDC), will be discussed as to their capabilities and their sequential historical development [1]. The high-frequency, thin-film calorimeters, capable of ultra-fast scanning (up to 10^6 K s^{-1}) and capable of giving information on a wide range of rates of fast thermal processes is described elsewhere in this MOTT Workshop [3].

Adiabatic calorimetry

With the development of the adiabatic calorimeter by Nernst, in 1911, the standard for high precision in calorimetry was reached [4]. Errors in determination of heat to an error of less than 0.1 % are possible, depending somewhat on temperature range and type of sample. Figure 1 shows an example of such a calorimeter constructed in the 1950s for the analysis of linear macromolecules [5]. This shown calorimeter documents the beginning of sophistication in the design of electronic controls, as summarized in [6]. Full computer control of instrumentation and data analysis is possible by now [7–9].

Using twin calorimeters offers advantages for certain applications where small differences between sample and reference need to be assessed [6]. Experience with the calorimeter of Fig. 1, however, revealed that twin calorimeters are difficult to control, and the gain in precision was small. A major expansion of the capability of the calorimeter was possible when running the calorimeter of Fig. 1 in a scanning mode of about 0.25 K min^{-1}. This allowed a separation of irreversible processes from the zero-entropy production response. It was then possible to investigate the melting range of semicrystalline polyethylene, bypassing much of the irreversible reorganization of the crystals [10]. Methods of increasingly fast [11] and, by now, superfast scanning [12] have led to successful elimination of ever faster processes [3]. Calorimetry better suitable for separating reversible from irreversible thermodynamic changes in the glass transition and melting ranges is described next.

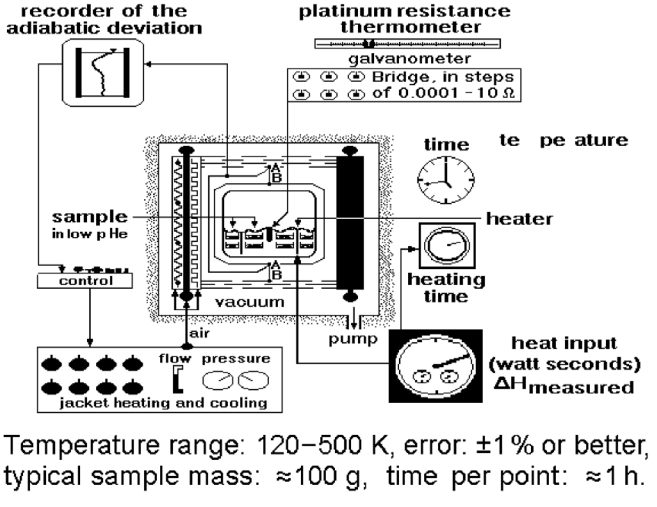

Fig. 1 Schematic of an adiabatic calorimeter, designed to measure heat capacities and heats of transition of polymers [5]. Note, for the measurement of heat it uses a direct watt-hour meter. The listed performance data apply to measurements of heat capacities and latent heats. At low temperatures, the controlled air-flow is cooled with liquid nitrogen or dry ice.

Standard DSC

The roots of DSC are found in simple cooling and heating curves produced since the 18th century as soon as reliable thermometers were invented [1]. Newton's law

$$dT/dt = K(T_o - T) \quad (1)$$

allows one to relate measured temperatures, T, to various thermal processes when inserting a sample into a surrounding bath of constant temperature, T_o. Over not too large temperature ranges, the constant K accounts for the nature, geometry, heat capacities, and thermal conductivities of the experimental set-up. Any change of the sample in heat capacity (or thermal conductivity) as occurring in glass transitions can be seen as a change in the slope dT/dt. Any latent heat will result in a slope of zero during the time interval needed for its conduction into or out of the sample.

When it became possible at the end of the 19th century to measure and record temperatures by thermocouples, differential thermal analysis (DTA) proved advantageous by producing traces of ΔT vs. time, t [13]. This new thermal analysis instrument could, at least approximately, be calibrated for quantitative calorimetry [14]. The early DTA made use of samples of approximately 1 g, but it was soon discovered that reducing the sample size allowed an increase in heating rate and was advantageous in achieving reproducible heat conductivity geometries as well as reducing heat losses [11]. By the 1970s, DTA had become a calorimetric technique, able to handle samples of 0.5–50 mg at heating rates of 50–0.5 K min^{-1} for the respective mass limits. It became customary to call the quantitative branch of DTA DSC [15]. Heat capacities could now be measured routinely and fast to ±3 % [16]. Figure 2 illustrates a design and the typical response of the DSC on imposing a constant heating rate q (= dT/dt) [1].

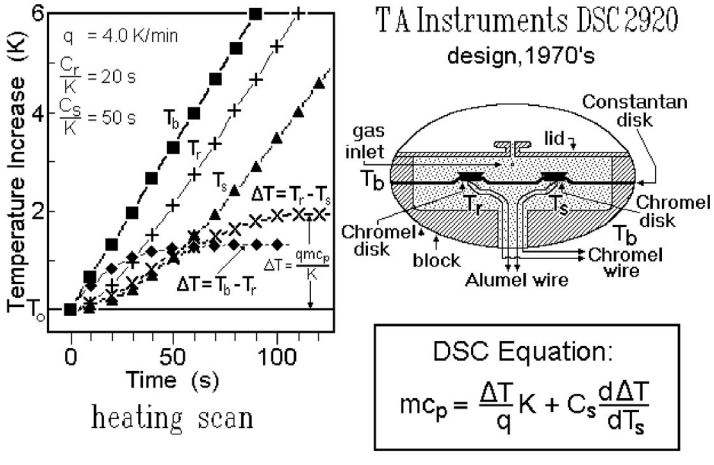

Fig. 2 Schematic of a DSC [1]. The graph shows the temperature profiles on start-up at the base (block), reference, and sample positions, T_b, T_r, and T_s. The total heat capacities of reference with pan and sample with pan are C_r and C_s. The heating rate is kept constant at $q = dT_b/dt$. The specific heat capacity of the sample, c_p, is given by the first term of the DSC equation with a small, second correction term (m = sample mass, the order of magnitude of the correction is 1–5 %).

The key issue in all calorimetry, and particularly DSC, is the calibration (i.e., evaluation) of the constant K in the variously applied Newton's law of eq. 1. Figure 3 illustrates the evaluation of heat capacities using a sequence of three runs between $t = 0$ and t_f. The need for identical initial and final isotherms and baselines is often neglected and leads to increased errors. The temperature range for a quantitative DSC is limited to a linear baseline and closely similar initial and final amplitudes for all

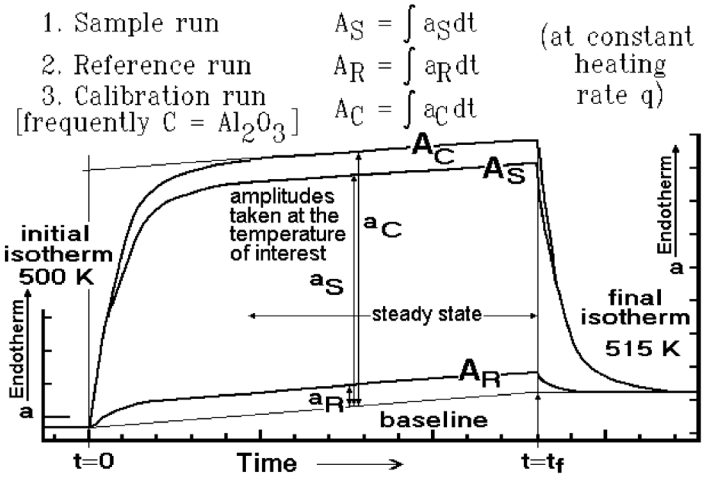

Fig. 3 Calibration of data from a standard DSC of the type shown in Fig. 2 [1]. The letters "A" represent the indicated areas, the letters "a", the corresponding amplitudes. Note that this analysis is valid as long as isotherms and baselines of the runs are identical within the expected precision.

isotherms. In modern DSC, this range can easily be 50 K, but it is rarely more than 100 K. Also, it must be considered that before the amplitudes of the heat-flow rates, a, reach steady state, they cannot be used for computation of the heat capacity. Furthermore, it must be established that the area lost on initial attainment of steady state and the area gained on approach to the final isotherm are in reasonable agreement. Only the full area A_S, after correction with A_R, corresponds to the total heat flow into the sample. In modern, commercial instrumentation, this correction is often taken over by computer programs based on an approximate model and a one-time calibration [17]. Although such one-run measurements save time, frequent checking of the applicability of the model used and of the constancy of the calibration is at the heart of the quantitative DSC [1,18].

TMDSC

A variation of the mode of running a standard DSC was developed in the 1990s by introducing a periodic temperature fluctuation. In Fig. 4, a TMDSC using a single-frequency, sinusoidal, modulation of the body temperature, T_b, is shown together with its sample temperature response, T_s, and the equation for the evaluation of the heat capacity [1,19]. The details of the operation of the calorimeter and the derivation of the TMDSC equation are given in [20,21]. Note that with proper programming, any standard DSC, as in Fig. 2, can be run as a TMDSC. In turn, as long as there are no major changes in the temperature lags during modulation, the sliding averages of temperatures and temperature differences over one modulation period (called the total quantities and marked by angular brackets < >) can be used as in a standard DSC analysis of Fig. 2, and indicated in Fig. 4.

Figure 5 illustrates the attainment of steady state in DSC at three constant values of q and the attainment of repeatability with the oscillating $q(t)$ in TMDSC [22]. As seen already in Fig. 2, DSC quickly reaches a steady state in heat-flow rate or ΔT, which then changes slowly with the changing heat capacity. The TMDSC, in contrast, reaches a repeatability later into the modulations and may never reach a truly steady state because of the varying $q(t)$. Under the chosen conditions, the observed heat-flow rates of DSC and TMDSC agree reasonably well. At higher amplitudes and frequencies, special calibrations are necessary, as discussed next.

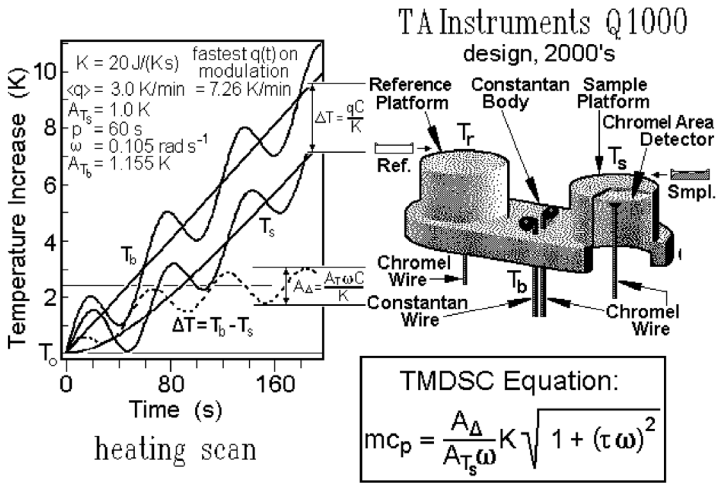

Fig. 4 Schematic of a TMDSC [1] with calculated temperature profiles (compare to Fig. 2). The underlying heating rate, <*q*>, is the sliding average over one modulation period. The modulation amplitude is expressed by A_{T_b} and the modulation period by *p*. The frequency is ω, and τ is a time constant which is sample- and mass-dependent. At high frequency, τ depends on ω.

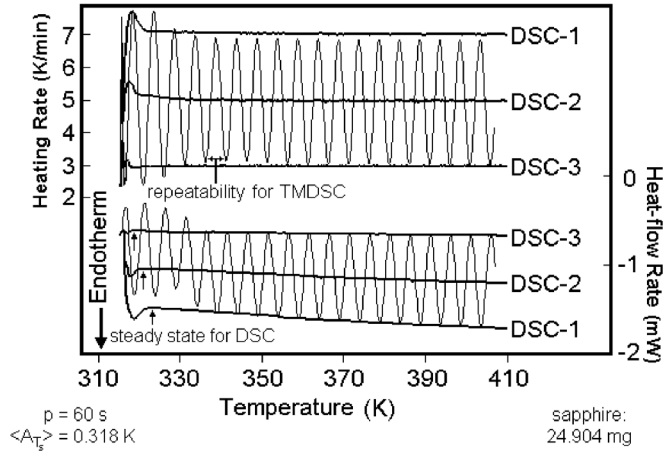

Fig. 5 Instantaneous heating rates and heat-flow rates for TMDSC and DSC [22]. The three DSC experiments were chosen to match the underlying <*q*> (2), the instantaneous *q* of the TMDSC at its maximum (1) and minimum (3).

Typical results for the measurement of heat capacity on a fast responding system modulated by a sawtooth oscillation are illustrated in Fig. 6 [23]. The standard DSC and TMDSC data in the left-hand graph were generated with the same calorimeter at the same time. The DSC data were obtained using eq. 1 of Fig. 6 during the end of the sawtooth modulation, just before the heating rate was switched. This is the time when steady state is most likely achieved. As can be guessed from Fig. 5, under these conditions the standard DSC keeps steady state to shorter modulation periods, *p*, than the TMDSC. The different amplitudes on TMDSC show little effect on heat capacity under the chosen conditions. The reversing heat capacity by TMDSC is initially calculated with eq. 2 of Fig. 6, assuming $K' = 1$. The TMDSC results deviate for periods shorter than 150 s. These data from short periods, however, can be corrected with an experimentally evaluated τ, as suggested by eq. 3 of Fig. 6, the same equation as shown in Fig. 4.

$$C_s - C_r = \frac{HF}{q} \quad (1) \qquad mc_p = \frac{A_{HF}}{A_{T_s}\omega} K' \quad (2) \qquad K' = \sqrt{1 + \tau(m)^2 \omega^2} \quad (3)$$

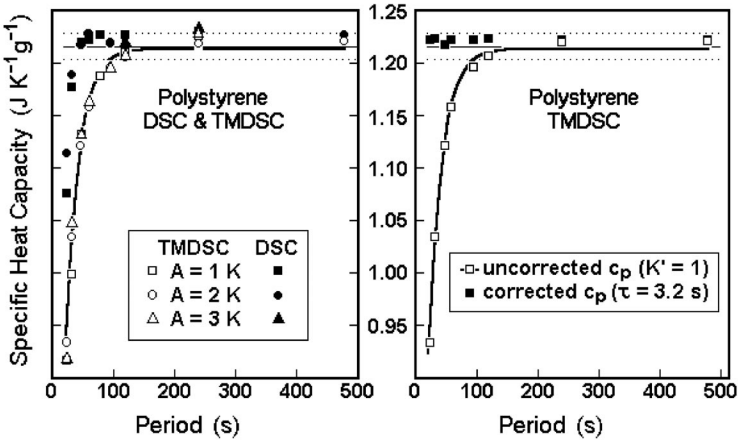

Fig. 6 Comparison of DSC and TMDSC data obtained with the same calorimeter (Perkin-Elmer DSC 7) [23]. The equations at the top correspond to the standard DSC analysis as in Fig. 2 (1) and the TMDSC analysis with $K' = 1$ (2), and fitted to expression 3 with a constant τ, as suggested in Fig. 4.

Additional details of the data treatment and the use of the multiple harmonics of the sawtooth modulation are illustrated in Fig. 7 [24]. Obviously, there are limits to the constancy of τ, which is equal to the slope in the lower left graph. It is possible, however, to fit the calibration curve in the lower left graph beyond the initial, constant slope and use a wider range of simultaneous modulations to obtain high-precision heat capacities. As one would expect, the three calibration runs shown in Fig. 3 result in different values of τ. With the (cumbersome) calibrations of Fig. 7, it became possible to achieve errors in heat capacity of less than 1 % with several different calorimeters of the power compensation and heat

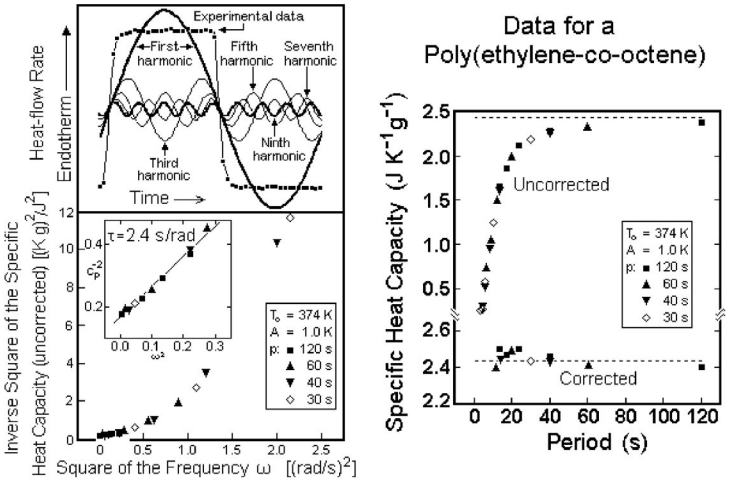

Fig. 7 Heat-flow rate as obtained by multi-frequency TMDSC arising from sawtooth modulation (upper left). The strongly period-dependent, uncorrected data on the right can be corrected with an approximately constant τ up to a period of 12.6 s (a frequency of 0.5 rad s^{-1}). At higher frequency, τ is not constant, but can be calibrated (see lower left) [24].

flux type [25–27]. The TMDSC approached the precision of adiabatic calorimetry. Considering this possible precision and the success of single calibration operation [18], one may consider making use of the experience of adiabatic calorimetry and constructing single-cell calorimeters for TMC.

Compared to adiabatic calorimetry, DSC and TMDSC can easily be constructed to reach higher temperatures. Most commercial DSCs reach 1000 K, and some can be used above 2500 K [1]. It is also possible to increase the heating rate for the scanning calorimeters by decreasing the sample size. In a typical DSC configuration, a 1-mm-thick polymer sample of 20 mg (for a disc of a radius 2.5 mm), for example, can be heated with 10 K min^{-1} without exceeding an internal temperature gradient of ≈0.6 K. Such gradients are acceptable for quantitative calorimetry. Extrapolating to thinner films, one expects similar performance from a 10-µm film heated with 10^5 K min^{-1} ($\approx 2 \times 10^3$ K s^{-1}). A film of 10 nm thickness, as seen in typical single lamellar polymer crystals, should be analyzable with rates up to 10^9 K s^{-1} without undue internal temperature gradients [11]. Commercial DSCs claiming 500 K min^{-1} heating rates have become available, and thin-film calorimeters which routinely reach above 10^6 K s^{-1} may soon become commonplace [3].

Quasi-isothermal TMDC

Besides the ability to produce quantitative calorimetric data, the basic mode of modulation can be varied, as outlined in Fig. 8 for the example of a single, sinusoidal frequency. Normal TMDSC is illustrated in the six upper examples (compare to Fig. 5). The top four curves result in TMDSC with continuous, though modulated, heating or cooling. No earlier reached temperatures are visited again as is possible for the bottom modes. The applications of the top modes of modulation are useful to exclude repeated, reversing, or reversible recrystallization or remelting. The seventh mode of modulated calorimetry at the bottom of Fig. 8 is, however, central. It represents the quasi-isothermal TMDC. This is the central technique discussed in this review and was proposed shortly after TMDSC became available [20,21]. The underlying heating rate, <*q*>, is equal to zero, keeping a constant average temperature, T_o. The modulation amplitude can be varied, so that truly isothermal calorimetry of reversible processes at chosen frequencies is possible by extrapolation to zero amplitude. In addition, TMDC can be extended to very long times (hours and days).

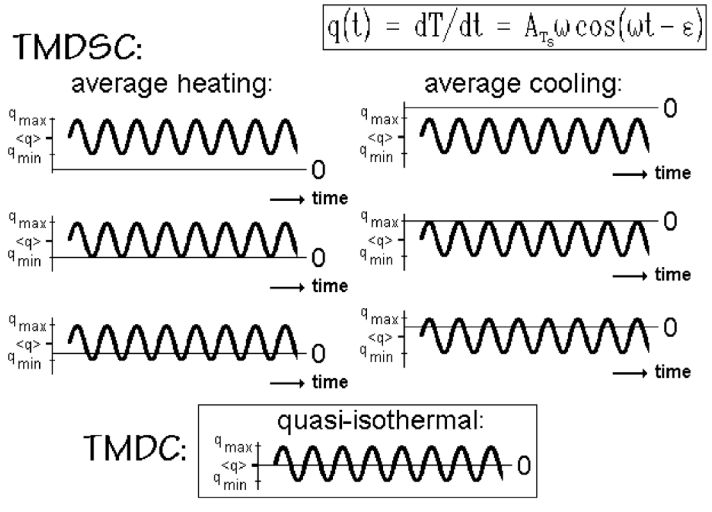

Fig. 8 Modes of operating TMDSC [1]. The bottom mode represents quasi-isothermal modulation (TMDC). The equation links temperature modulation with heating rate $q(t)$. The phase lag is given by ε.

To describe the overall change in enthalpy (H, heat content) caused by the heat flux into any calorimeter, one may start with the basic differential equation

$$dH = (\partial H/\partial T)_{p,n}\, dT + (\partial H/\partial n)_{p,T}\, dn \tag{2}$$

where the first partial differential, $(\partial H/\partial T)_{p,n}$, represents the thermodynamic heat capacity, C_p, at constant pressure, p, and composition, n. The second partial differential, $(\partial H/\partial n)_{p,T}$, represents the latent heat, L, at constant pressure, p, and temperature, T. The equation applies without restrictions as long as the system remains in equilibrium over the ranges of T and n investigated.

Many analyzed systems, however, show a slow response in heat capacity, as in the glass transition region. The first set of examples will deal with such applications. Other systems may undergo changes in composition, n, with a slow kinetics, as frequently encountered during chemical reactions and order/disorder transitions of semicrystalline, flexible, linear macromolecules. The second set of examples will show the treatment of order/disorder transitions. In the first case, a time-dependent heat capacity must be introduced in eq. 2, in the second, a time-dependent latent heat. To still get some useful thermal information, the calorimetry can be carried out either sufficiently slowly so that all changes in H go to completion within the time scale of measurement, or sufficiently fast, so that the system stays metastable. Otherwise, the effect of time must be included in one or both terms of eq. 2.

Outside the glass transition range, the thermodynamic heat capacity reaches equilibrium very quickly relative to the calorimeter response and is time-independent. Any lag due to the latent heat kinetics can then be dealt with by analyzing the second term in eq. 2, as long as lags due to thermal conductivity have been corrected for. The measured C_p is then an apparent C_p, $C_p^{\#}$

$$C_p^{\#} = dH/dT = (\partial H/\partial T)_{p,n} + (\partial H/\partial n)_{p,T} \times dn/dT \tag{3}$$

in which the change in composition with temperature, dn/dT, is not going from one equilibrium state to the other, but is determined by its temperature-dependent kinetics, and can be written as

$$dn/dT = (dn/dt)/(dT/dt) \tag{4}$$

The temperature-dependent kinetics of the system, dn/dt, and, the heating rate, q (= dT/dt) must now be evaluated separately.

Methods to derive the kinetics from the frequency dependence of TMDSC have been proposed, but are not part of this review. It was possible, for example, to establish a kinetic model of the mechanism of melting, crystallization, and recrystallization and apply it to the irreversible melting process of semicrystalline nylon 6. After calibration and separation of all other time-dependent effects, a single Debye-type relaxation could approximate the imaginary and real contributions to the complex, apparent heat capacity in a Cole–Cole plot of the frequency and heating rate dependence [28,29].

TIME SCALES OF THERMODYNAMIC EFFECTS AND MOLECULAR MOTION

It was stated at the beginning of the first section of this review that heat has its microscopic origin in molecular motion. This molecular motion, thus, must provide the cause of the time dependence of the calorimetric results. Two types of molecular motion can be separated: (1) oscillations of small amplitudes, and (2) large-amplitude motion which, depending on the state of matter and type of molecules, includes translational, rotational, and conformational motion (= internal rotation). The first two large-amplitude motions involve the molecules as a whole, the third involves rotations of parts of the molecules, causing flexibility of the molecules (conformational changes). For flexible, linear macromolecules, the central type of material described in this review, the large-amplitude motions are almost exclusively conformational.

A single atom, free or part of a molecule, has three degrees of freedom, distributed over the various types of motion. A macromolecule of, let us say, 100 000 atoms has then 300 000 degrees of freedom. This large number of different possible motions must be assessed to understand the basis of the

thermodynamics of polymers. For vibrational motion, the basic link to the heat capacity at constant volume, C_v, was established at the beginning of the 20th century and is known as the Einstein function [30]. Their influence on the thermal properties in the condensed states is summarized next [1].

Link of heat capacity to vibrational motion

In the solid state at sufficiently low temperature, all molecular motion is vibrational. When discussing the possible vibrations in crystalline metals and salts, it was recognized that the vibrations of each atom are determined mainly by the force field of its 6–12 symmetrically placed neighbors. Initially, it was assumed that such a symmetric force field may be approximated by spherical symmetry which yields the same frequency for each degree of freedom [30]. Comparison with the results of adiabatic calorimetry revealed that at intermediate temperatures this assumption was valid, but at the lowest temperatures, the calculated heat capacity was too high and the single frequency had to be replaced by a distribution which also had to account for the low acoustic frequencies known from vibrating solids. The problem was resolved by replacing the single Einstein function by a three-dimensional Debye function, derived from the description of acoustic vibrations, extended to higher frequencies until the maximum number of degrees of freedom were accounted for [31]. This treatment accounted for the heat capacities of many metals and salts over wide temperature ranges by specifying only the end-frequency of the distribution, $\nu_{(\mathrm{Debye})}$, the three-dimensional Debye temperature Θ_3 (= $h\nu_{(\mathrm{Debye})}/k$, in kelvin, h = Planck's constant, k = Boltzmann's constant) [32]. For lamellae, the strongly bound molecular structure deviates from three- to two-dimensional. An example of such a substance is graphite. For one-dimensional, linear structures, such as in linear macromolecules, the Debye function must be adjusted to one-dimensional symmetry. Empirical equations for these cases were suggested by Tarasov [33], based on one- to three-dimensional Debye functions. Even more complications are introduced by local modes of vibration, commonly called group vibrations. These vibrations do not couple throughout the solid, but can be assessed by IR and Raman spectroscopy and their narrow distributions can then be converted to heat capacities by using single Einstein functions or simplified distributions of frequencies.

An example of a fit of the frequency spectrum of crystalline polyethylene [34] to its heat capacity is shown in Fig. 9 [35]. The skeletal vibrations can be approximated by a combination of one- and three-dimensional Debye functions, as suggested by Tarasov [33]. They account for only two modes of vibration per CH_2-group, the torsional and longitudinal vibrations, coupling in a one- and three-dimensional fashion, as indicated by the Θ-temperatures in Fig. 9. Up to 150 K, the C_v ($\approx C_p$) is almost fully accounted for by these skeletal vibrations and calorimetry permits an easy fit to the approximate frequency spectrum.

The additional contribution of the seven group vibrations accounts for the heat capacity at higher temperatures. For their calculation, no further calorimetric input is necessary, except for the evaluation of $C_p - C_v$ which, however, can also be approximated from empirical knowledge when data on expansivity and compressibility are unavailable [36].

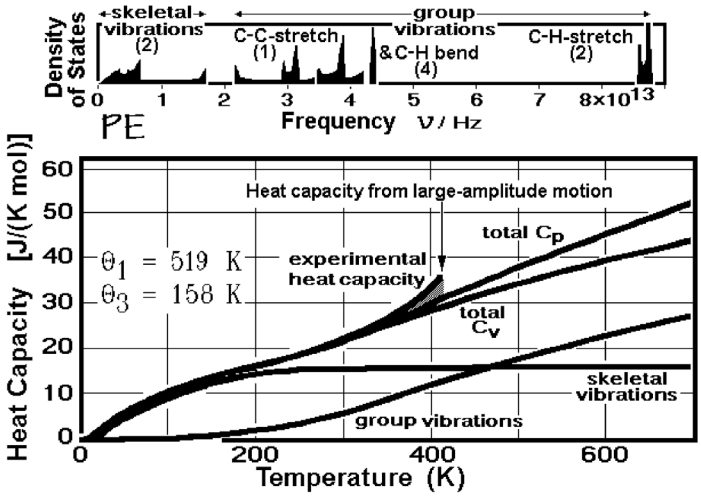

Fig. 9 Heat capacities C_p and C_v of crystalline polyethylene per mole of CH_2 as they relate to the vibrational densities of state [1]. Note the additional contribution from the large-amplitude motion to the heat capacity of the crystals with a melting point of $T_m{}^o = 414.6$ K.

ATHAS Data Bank

When sufficient data on heat capacities of linear macromolecules were measured [37] and their link to the vibrational motion established, it was possible to generate reliable extrapolations of the thermodynamic properties in equilibrium and in metastable states. Figure 10 shows such data for polyethylene. The frequency spectrum at the top of Fig. 9 reveals that the vibrations below 10^{12} Hz, with a time scale above one picosecond (10^{-12} s), are negligible with respect to their contributions to the thermodynamic functions in Fig. 10. This means that in calorimetry, the heat capacity of the solids reacts instantaneously to changes in temperature.

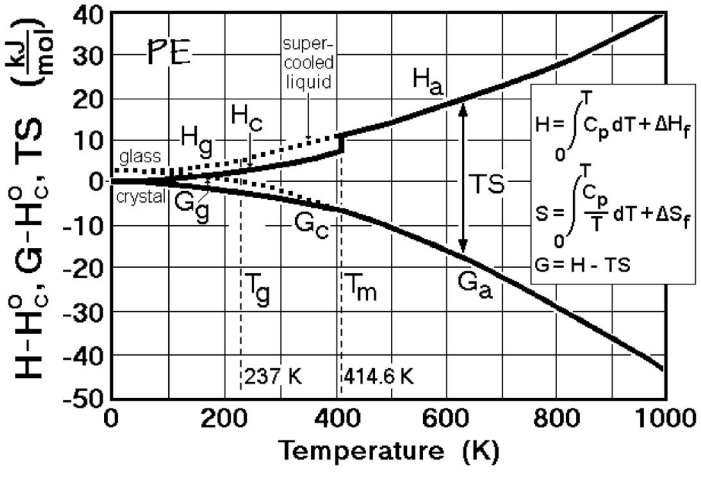

Fig. 10 The integral thermodynamic functions H, S, and G of crystalline (c), liquid-amorphous (a), and glassy (g) polyethylene [1]. Also shown are the glass and melting transition temperatures, T_g and T_m, and the equations linking them to the heat capacity.

In the 1980s, the classical depositories of thermodynamic data did not accept data on polymers. It was thought, erroneously, they did not meet the standards of equilibrium substances. To overcome this problem, the ATHAS Data Bank of "Heat Capacity and Other Thermodynamic Properties of Linear Macromolecules" was generated in the 1980s and updated in 1991 [38].

Figure 10 combines the heat capacity information available from low-temperature calorimetry of solid polymers with data from liquids. Between the glass transition and the melting temperature, the vibrational C_p can be safely extrapolated, as shown in Fig. 9. In addition, it was found that below the glass transition, all solid phases of the same polymer are close to having the same heat capacity down to about 50 K. The somewhat higher heat capacities of the glasses result in a lower Θ_3 temperature at lower temperature. For polyethylene, the glassy Θ_3 is 80 K, compared to 158 K of the crystals (Θ_1 is identical for both).

About 200 linear macromolecules and related smaller molecules are at present listed in the ATHAS Data Bank, including all poly(amino acid)s, some of their copolymers, and a number of proteins [37]. Because of the great similarity of the weak intermolecular forces in polymers and the strong C,N,O backbone-bonding, this database with an overall error of ±3 % can be used to estimate the heat capacities of samples which have not been measured. This is particularly valuable for the unlimited numbers of proteins and synthetic copolymers [1]. Above the glass transition, semicrystalline macromolecules, being metastable, may become unstable with increasing temperature. On approach of the melting temperature, for example, a multitude of reorganization, irreversible melting, and recrystallization may occur. These effects cause changes in $C_p^{\#}$ of eq. 2 with a much longer time scale than the fast vibrations with their frequencies of more than THz (10^{12} Hz), shown in Fig. 9 for polyethylene. For the interpretation of the measured data, they must be compared to the thermodynamic functions caused by vibrations-only, which represent the hypothetical equilibrium crystal in Fig. 9.

LINK TO LARGE-AMPLITUDE MOTION

Conformational rotation, the basic large-amplitude motion of linear macromolecules, can be simulated in crystals using large-scale molecular mechanics calculations [39]. In these simulations, the main local internal rotation involved three backbone bonds, causing 2g1 defects with two gauche bonds separated by one trans bond. At room temperature in polyethylene-like crystals, such defects have a lifetime of the order of magnitude of 10^{-12} s and a concentration of 0.5 %. The calculations substantiated earlier proposals based on matching the deviations of the heat capacity from the vibration-only value, as seen in Fig. 9 [40], and also concentrations of gauche conformations measured by IR spectroscopy on paraffins [41]. The effect of an isolated, internal rotation at low temperature is similar to a torsional vibration. At higher temperature, when the barrier to rotation can be overcome, it reaches a maximum in heat capacity and finally drops to the limit of a rotator to half the vibrational heat capacity [42]. In the presence of the close packing in the solid state, the rotations become cooperative in nature. The multichain process increases the relaxation time to values reaching the measurable effects by DSC and TMDSC. Detailed model calculations made use of Eyring's hole model [43], which describes the overall configuration involved in the large-amplitude conformational motion by a volume with 1 nm or smaller radius, centered about a "hole".

Figure 11 shows a comparison of the heat capacity contribution of the large-amplitude motion in glassy polyethylene to that of crystalline polyethylene, shown also in Fig. 9 [44]. The beginning of the glass transition in amorphous polyethylene displays a similar increase to the conformational effect in the crystal, just that the motion starts instead of room temperature at 120 K. Such a shift is expected for the less dense packing in the glass and its lower Θ temperature. Besides this time-dependent heat capacity effect which affects the first term on the right-hand side of eq. 3, a much larger kinetic effect is expected from the latent heat connected with the second term. If the latent heat is connected to an order–disorder effect, as illustrated in the examples of the next section, the kinetics involves nucleation and growth kinetics, usually classified as a first-order process [45]. Underlying the first-order processes

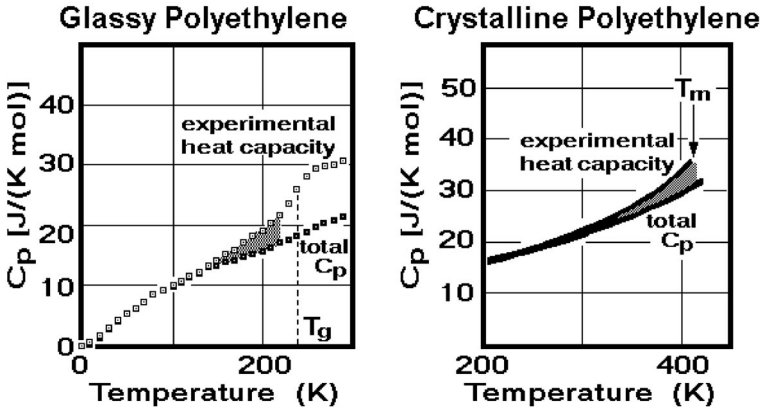

Fig. 11 Comparison of the heat capacity contribution of the large-amplitude motion in crystalline polyethylene (right) to that of glassy polyethylene (left) [44].

are, however, also changes in heat capacity as during the glass transition. For flexible molecules, these changes in C_p involve large-amplitude, conformational motion. Calorimetry, thus, deals frequently simultaneously with more than one type of kinetics.

EXAMPLES OF THE REVERSIBLE AND IRREVERSIBLE PROCESSES

Glass transitions will be the first examples of reversible and irreversible thermodynamic changes studied with the various types of calorimetry described in the first section of this review. This will be followed with examples of combinations of the glass transition with order–disorder processes. In all cases, measurements of apparent heat capacities will be judged against the contributions of the fast vibrations to the reversible C_p, as discussed in the second section.

Glass transitions of polystyrene (PS) and poly(ethylene terephthalate) (PET)

The cooling rate dependence of the glass transition of PS was followed over 40 years ago by DTA. In order to achieve higher precision in the assessment of T_g, a thermocouple was directly embedded into the sample [46]. Figure 12 illustrates the results and also shows the good agreement of a representation of the data when fitting with the hole model of Hirai and Eyring [43]. The exponential curve suggests that infinitely slow cooling may retain the heat capacity of the liquid to absolute zero. Naturally, such experiments are impossible to conduct. But also, it is erroneous to extrapolate the heat capacity of the liquid to temperatures below T_g to assess the thermodynamic functions of a hypothetical liquid below T_g. Such extrapolation keeps a higher C_p of the liquid than the solid and results ultimately in a higher entropy than that of the crystal, the so-called Kauzman paradox [47]. With better estimates of the C_p of the liquid, it could be shown recently that, at least for polyethylene, this paradox does not exist [48]. Even when avoiding the glass transition (as expected on infinitely slow cooling), the heat capacity of the liquid should drop sufficiently quickly to that of the solid to yield a positive entropy at 0 K.

The next step to analyze the glass transition involves TMDC. Figure 13 illustrates a series of points generated for PET of different thermal histories and crystallinity [49]. The TMDC data were taken during the last 10 min of a 20 min run (p = 60 s). This time before data collection was long enough to reach repeatability and cause the overall drift of the sample toward equilibrium to be negligible. The modulation was properly chosen so that the Lissajous ellipse of a plot of sample temperature vs. heat-flow rate was constant and symmetric over these last 10 modulation cycles and generated 200 reproducible data, averaged for each T_o. The sequence of measured runs of the temperatures T_o in Fig. 13

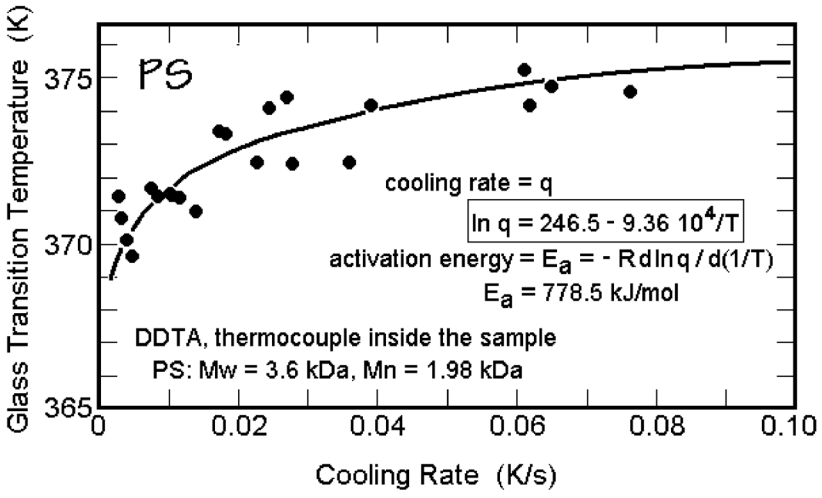

Fig. 12 The glass transition of PS as a function of cooling rate, measured with DTA by finding the half-change of heat capacity on going from the liquid to the glassy state [46].

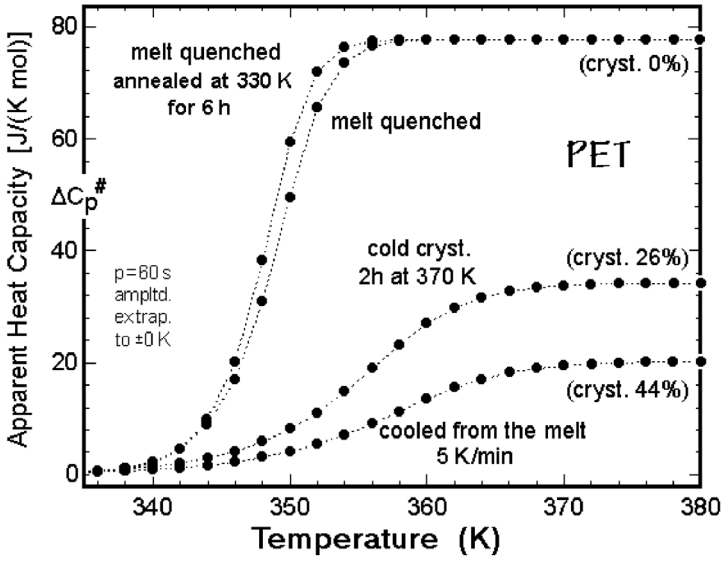

Fig. 13 Change of heat capacity of amorphous and semicrystalline PET in the glass transition region as measured by TMDC [49].

could be performed on cooling and heating with identical results. Finally, frequency data of different amplitude were extrapolated to zero amplitude, to reach the true change in C_p with frequency. Analyzing the different samples with a simple, first-order kinetics, based on the hole theory or irreversible thermodynamics [50,51], yielded different relaxation times, accounting for the broadening of the transition when going from amorphous, annealed glasses to slowly cooled, semicrystalline samples. In addition to the broadening, the change in heat capacity through the glass transition was not linear with the crystallinity (measured from the latent heat of fusion), rather it suggested a sizable amorphous fraction that does not participate in the measured glass transition. This fraction remains rigid on heating and shows a separate glass transition at higher temperature. It was identified as a rigid-amorphous

fraction (RAF) of nanophase dimension. Both crystallinity and RAF, thus, must be known to judge the mechanical properties of semicrystalline polymers.

Figure 14 gives additional details about the TMDC in the glass transition range of a fully amorphous PS [52], analyzed in the same fashion as the PET of Fig. 13. The left-hand figure shows the data for three different periods, *p*, matched to amplitudes so that the maximum and minimum heating rates of all frequencies are identical. The right-hand figure illustrates the change in the apparent heat capacity over a wider frequency range, calculated from the data on the left [50]. Several different responses can be understood from the chosen simplified model. The three most surprising effects on the resulting heat-flow rates are the following: (1) a small, constant contribution, (2) a second harmonic contribution, besides the main first harmonic response, and in addition, (3) a frequency shift of the main, first harmonic response which is then not identical to the modulation frequency anymore. All effects need to be considered to interpret the heat capacity properly.

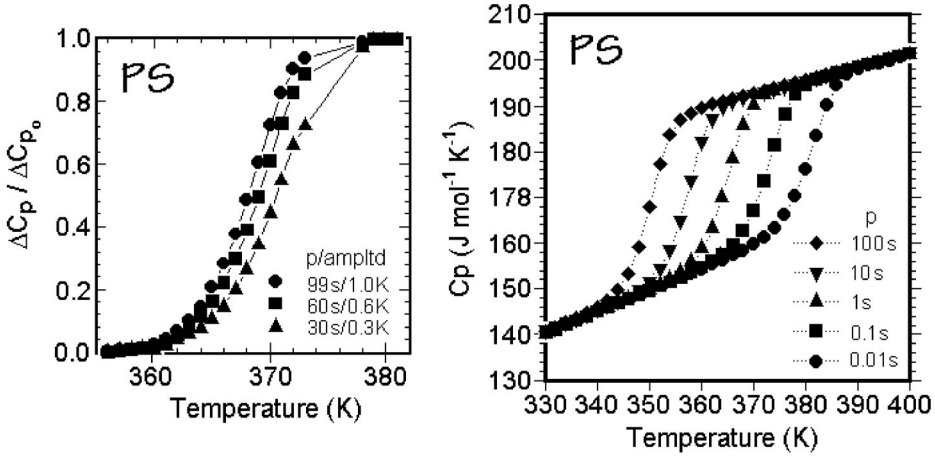

Fig. 14 Glass transition of PS. Left, measured at different periods and amplitudes [52]. Right, recalculated to a wider frequency range using the hole theory of glass transitions [43,50].

Glass transition of poly(oxy-1,4-2,6-dimethylphenylene) (PPO)

The next example of TMDC is the glass transition behavior of semicrystalline PPO, represented by Fig. 15 [53]. Following the standard DSC trace, one finds that below the beginning of melting, all amorphous PPO on the sample must belong to the RAF. There is no indication of a lower glass transition as in semicrystalline PET. The melting of PPO is completely irreversible, no contribution is detectable in the TMDC trace. Comparing the RAF (from TMDC) and the crystallinity (from DSC), one can see the change in C_p at the beginning of the melting peak is largely due to the glass transition of the RAF. When major melting starts, every three RAF repeating units going through their T_g allow melting of one crystalline repeating unit. The TMDC, thus, reveals a completely different picture of the melting of PPO, a common commercial polymer, from that normally assumed. The melting is fully governed by the RAF surrounding the crystals. Only when the RAF becomes mobile, can the crystal melt. The melting kinetics is fully determined by the kinetics of the glass transition. These novel properties can account for the different behavior of PPO compared to other semicrystalline polymers. Trying to anneal PPO below the melting peak reduces (!) the crystallinity, and because of the RAF formation, no crystallization is observed on cooling from the melt.

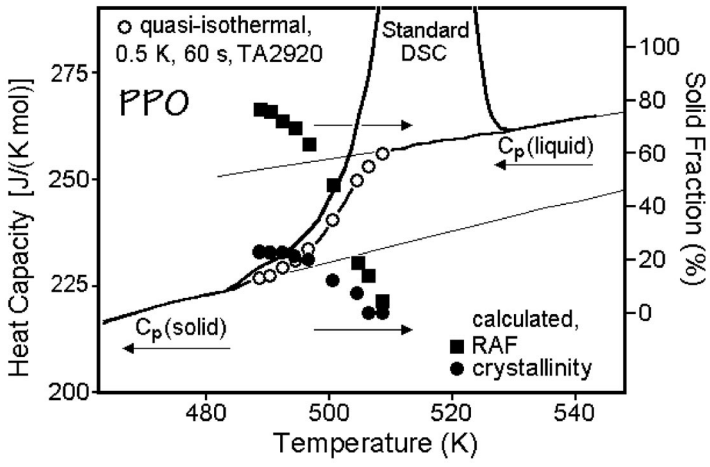

Fig. 15 Analysis of semicrystalline PPO with TMDC and DSC. The apparent heat capacity curves show a full separation of the latent heat measured by DSC and the underlying glass transition by TMDC. The solid fractions due to crystallinity are calculated from the latent heat by DSC, and the glass transition of the RAF is calculated from the TMDC [53].

TMDSC of the reversible and irreversible melting of In

A much bigger kinetic effect is observed in the melting region of other semicrystalline polymers. Before the TMDSC and TMDC experiments became available, it was thought that equilibrium melting and crystallization were only possible in the presence of remaining crystal nuclei and for rather small molecules. The flexible linear macromolecules were expected to melt irreversibly due to the need of molecular nucleation [1]. A larger number of TMDSC experiments have been reviewed recently and are a resource of examples of reversible crystallization, even in semicrystalline macromolecules [54].

Indium, the typical reference substance for DSC, can serve as an example of the normal melting behavior. Figure 16 shows the classical melting of In [55]. The first time the melting temperature is reached beyond the maximum temperature of the previous cycle is with peak 1. There is, however, insufficient time to melt the sample completely. Only between peaks 7 and 12 are melting and crystallization separated within the modulation cycles. This is followed by incomplete crystallization. A nucleation effect of the crystals is only detectable on TMDSC on cooling from the melt. One must assume that the temperature gradient within the sample keeps some nuclei under the modulation conditions of Fig. 16. More details are available from TMDC with modulation amplitudes of 0.05 K and steps of T_o of 0.10 K. With such TMDC, the melting temperature could be fixed to within 0.02 K. It is clear from Fig. 16 that the kinetics of melting requires the separation of instrument lag from the measured time effect, possible only with TMDC.

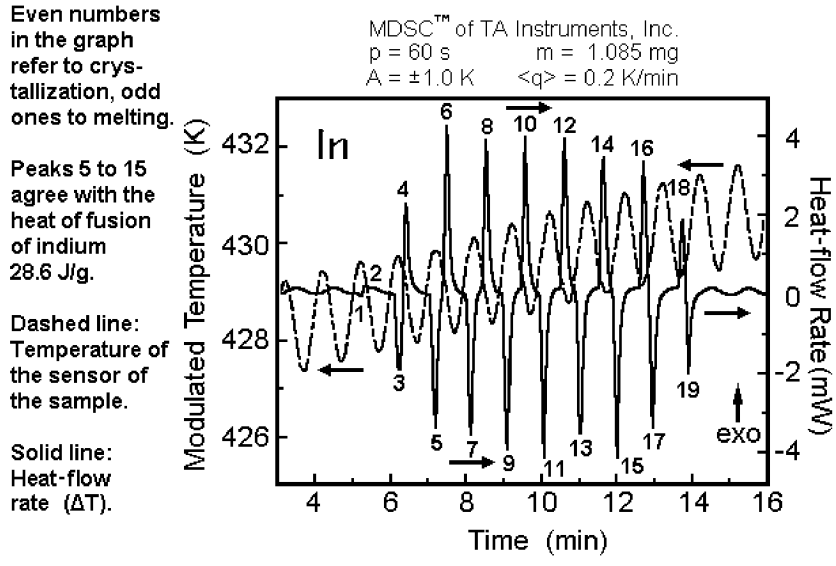

Fig. 16 Melting of In by TMDSC on heating, showing multiple melting and crystallization as long as the temperature modulation covers the melting and crystallization range [55].

Irreversible and reversible melting of poly(oxyethylene) (POE) and the transitions of its crystals

The melting of macromolecules was expected, as mentioned in the section on PPO, to be irreversible. Figure 17A shows an example of DTA and TMDC of a well-crystallized, low-molar-mass POE [56]. Indeed, the data seem to indicate fully irreversible melting. Going to much higher molar mass, the behavior changes. There seems to be a certain fraction which melts reversibly at 339 K, as illustrated with Fig. 17B [57]. The same has been found for a number of other semicrystalline polymers [54], suggesting a different, specific melting behavior for every polymer analyzed. In general, the poorer the crystals, the larger is the fraction of reversible melting. Fully irreversible melting is approached only for the best crystals and for increasingly more rigid molecules [54]. The proof of the truly reversible fraction in high-molar-mass POE is shown in Fig. 17C with a fully symmetric outer Lissajous figure at the reversible melting peak after more than 20 min of modulation [58]. The Lissajous figure showed no further change on extending the modulation time to 10 h. The inner Lissajous figure corresponds to the same sample in the amorphous state, reached by cooling from the melt, also to a T_o of 338.5 K. Due to the absence of nuclei on cooling from the melt, crystallization starts only at 331 K. By detailed analysis on several polymers, it was found that the reversible melting is a local process at the growth faces of the crystals, in agreement with Fig. 17C [54].

The analysis of POE with TMDC revealed one more unexpected property. Enlarging the heat capacity in Fig. 17A sufficiently and waiting for all melting to subside, one finds an increase of C_p from the level of the solid to that of the liquid occurring *below* the start of melting. This change of C_p indicates a broad glass transition and is documented with Fig. 17D. Following the crystal structure on heating by X-ray diffraction [58], there was no change in structure, only an increase in the lattice spacing. This is taken as proof, that in POE the crystal and glass transition do not occur simultaneously, but that T_g of the crystal of POE occurs approximately 20 K lower than T_m. This can be compared to PPO, where the crystals cause a surrounding, rigid amorphous phase, permitting melting only at a temperature above the T_g of the RAF (see Fig. 15).

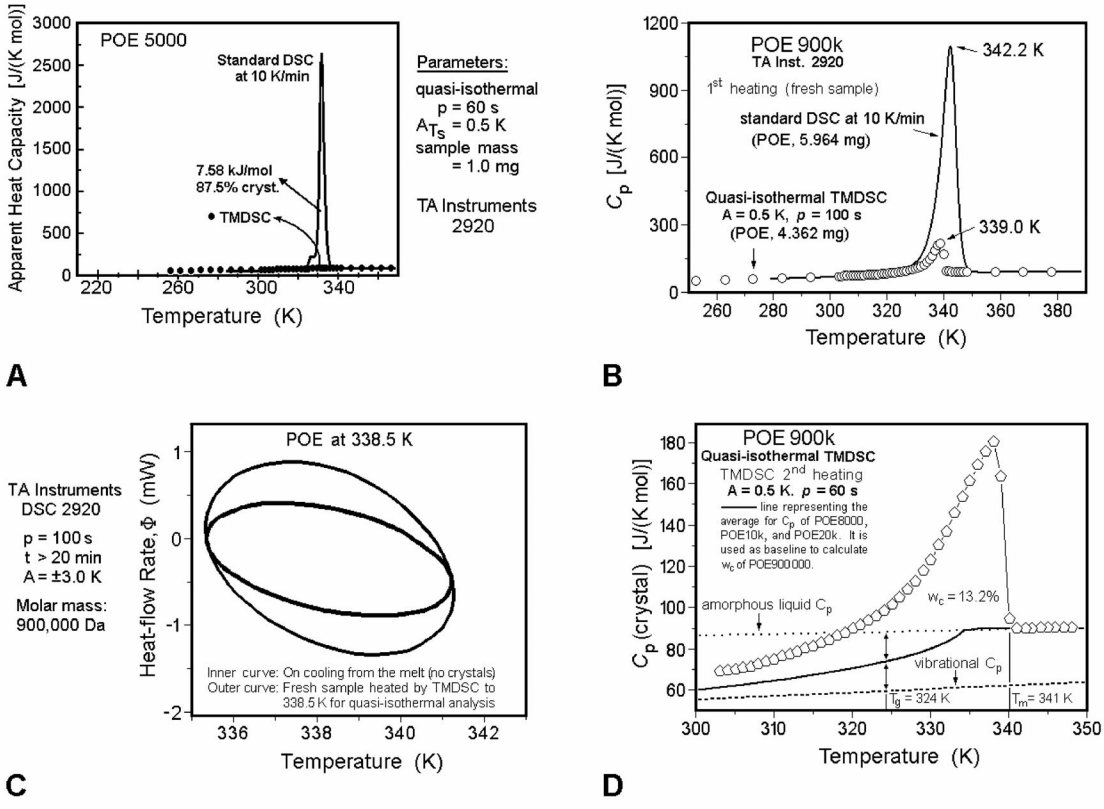

Fig. 17 Melting of POE by DSC and TMDC. A: Irreversible melting of a low-molar-mass sample of 5000 Da [56]. B: Melting of a high-molar-mass sample of 900 000 Da, showing a fraction of reversible melting [57]. C: Lissajous figure of the heat-flow rate response to the modulated temperature at 338.5 K, proving reversibility [58]. D: Details of the glass transition and the reversible melting of POE of molar mass 900 000 Da [58].

Transitions in poly(butylene terephthalate) (PBT) as separated by TMDC

An example of the analysis with DSC and TMDC of the two glass transitions and the local, reversible melting of the amorphous PBT is illustrated in Fig. 18. Only above 400 K can the overall heat capacity of the PBT be expressed by the common two-phase model as given by the listed equation in Fig. 18. The midpoint of the T_g of the RAF is at 375 K, accounting for 21.3 % amorphous nanophase enclosing the crystals [12]. The low-temperature glass transition at 314 K is linked to the fully amorphous bulk phase of PBT, which can be made by quenching from the melt. The standard DSC reveals the complicated reorganization and recrystallization in the melting peak. Quite clearly, again, TMDC enables detection of considerably more details about the transition region of PBT. Without this insight, it is not possible to develop the supporting science for industrial applications of this polymer.

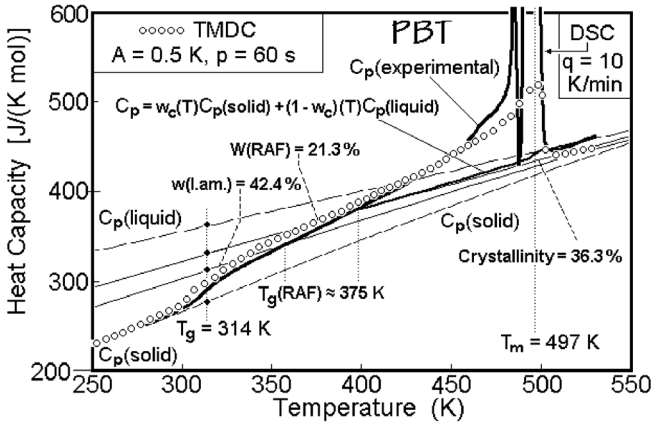

Fig. 18 TMDC and DSC of PBT [12].

Melting of the nylons as seen by TMDC

Nylons are a wide range of polyamides having seen extensive commercial applications since the 1930s. Studying the polyamino acids (nylon 2), one analyzes the base materials of proteins. It is thus surprising that these materials were not investigated in more detail calorimetrically. Superficially, the melting behavior of many nylons is similar to that of other synthetic polymers [54]. Standard DSC reveals a broad melting range. Some nylons, such as nylon 6.6, undergo within this broad temperature range the crystallographic Brill transition, a phase transition from the triclinic crystal to the pseudo-hexagonal structure of a mesophase. Basically, the nylons with longer CH_2 sequences have a crystal structure dominated by intermolecular, H-bonded planes which remain largely undisturbed until full isotropization. The CH_2 sequences, in contrast, are packed in an extended-chain structure. They are far above the melting temperature of paraffins of equivalent length, and even polyethylene. Direct measurement of the motion of the CH_2 groups with quasi-elastic neutron scattering and NMR revealed large-amplitude motion.

The details of the melting range could only be understood with recent TMDC. Figure 19 illustrates the TMDC starting from low-temperature T_g at 333 K involving about half of the amorphous fraction [59,60]. This is followed immediately with a second glass transition of 36 % RAF, centered at about 370 K. The filled squares of the expected C_p are calculated assuming 28 % crystallinity. The true reversible C_p, separated from all irreversible and slow melting processes, could be established by extrapolating the modulation from the measured 10-h-long TMDC experiments to infinity. One must assume that its further increase in C_p beyond that of the liquid is the beginning of the glass transition of the crystal, beginning at ≈400 K. At 435–455 K, the Brill transition is complete. In the pseudo-hexagonal phase, the C_p does not increase further relative to that of the liquid. This interpretation agrees also with the results from the X-ray diffraction [60]. Only at about 480 K does the mesophase begin its irreversible isotropization with a T_i of 534–545 K and possibly some reversibly decoupled chain segments on their growth face, which account for a small amount of reversible melting seen in Fig. 19.

These complicated processes of the nylons from 300 to 550 K leave many open questions, but TMDC provides a tool for further quantitative research. Lower-melting nylons than nylon 6.6, as for example nylon 6, do not reach the mesophase transition and may provide a simpler melting range. Figure 20 represents a schematic of the possible paths and properties for the isotropization when starting from solids with different degrees of molecular order at low temperature.

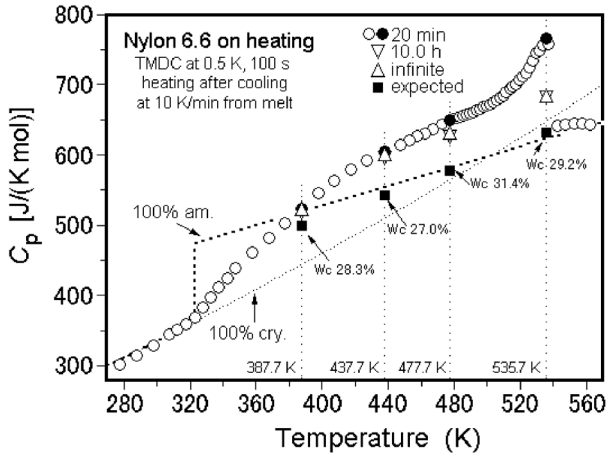

Fig. 19 TMDC of nylon 6.6 in the melting region [59].

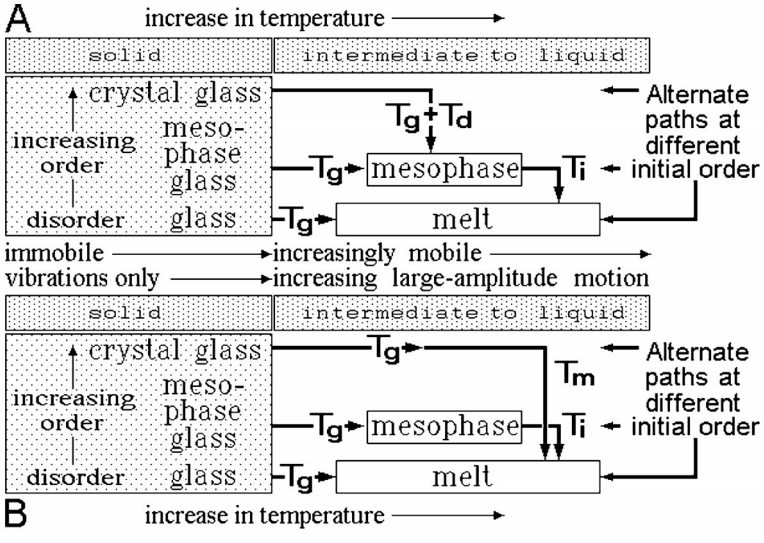

Fig. 20 Schematic of the transitions of the three types of glasses as found in nylon 6.6 (A) and nylon 6 (B). A: For the crystal glass T_g and T_d overlap and yield a Brill transition to the mesophase which, in turn, undergoes an isotropization at T_i to complete the melting. B: The crystal glass completes a glass transition T_g before melting at T_m without change in crystal structure [60].

CONCLUSIONS

The conclusions can be concentrated into four points: (1) Quasi-isothermal TMDSC, TMDC, coupled with standard DSC can be used to test the reversibility of thermodynamic transitions and can yield heat capacities to a precision of better than 1 %. (2) Links of C_p to vibrational and large-amplitude molecular motion and use of the ATHAS Data Bank allow the separation of the reversible C_p from latent heats using TMDC. (3) Single and multiple glass transitions can be investigated with TMDC, including rigid-amorphous phases of semicrystalline polymers and possible glass transition of crystals. (4) Reversible, partially reversible, and irreversible melting can be studied with TMDC. For example, both, perfect, metastable folded-chain and rigid, long-chain molecules show no reversible melting. Reversibility of nucleated crystallization can be analyzed and can clarify molecular nucleation.

ACKNOWLEDGMENTS

The ATHAS effort was supported by the Polymers Program of the Materials Division of the National Science Foundation and the Division of Materials Sciences and Engineering, Office of Basic Energy Sciences, U.S. Department of Energy at Oak Ridge National Laboratory, managed and operated by UT-Battelle, LLC, for the U.S. Department of Energy, under contract number DOE-AC05-00OR22725.

REFERENCES

1. For an extensive review of this topic, see: B. Wunderlich. *Thermal Analysis of Polymeric Materials*, Springer, Berlin (2005). See also the computer course *Thermal Analysis of Materials,* 2007, available online: <www.scite.eu> or <http://athas.prz.rzeszow.pl>.
2. See, for example: A. Lavoisier. *Elements of Chemistry*, Edinburgh (1790), translation of the *Traité élémentaire de Cemie*, Paris (1789) by R. Kerr, Part I, Chap. I. Available as facsimile reprint, Dover, New York (1965).
3. See: C. Schick. "High frequency thin film calorimeters in combination with ultra fast scanning", a paper presented at the workshop on "Modulated and oscillation temperature techniques" (MOTT), 20th International Conference on Chemical Thermodynamics, Warsaw, Poland, 3–8 August 2008; For superfast calorimetry, see also the proceedings of the 8th–10th Lähnwitz Seminars, *Thermochim. Acta* **432** (2005), **461** (2007), **492** (2009).
4. W. H. Nernst. *Ann. Phys.* **36**, 395 (1911).
5. A. E. Worthington, P. C. Marx, M. Dole. *Rev. Sci. Instrum.* **26**, 698 (1955).
6. (a) J. M. Sturtevant. "*Calorimetry", in Techniques of Chemistry*, Vol. I: *Physical Methods of Chemistry,* Part V: *Determination of Thermodynamic and Surface Properties,* A. Weissberger, B. Rossiter (Eds.), Chap. VII, John Wiley, New York (1971); (b) B. Wunderlich. "*Differential thermal analysis"*, in *Techniques of Chemistry*, Vol. I: *Physical Methods of Chemistry,* Part V: *Determination of Thermodynamic and Surface Properties,* A. Weissberger, B. Rossiter (Eds.), Chap. VIII, John Wiley, New York (1971).
7. E. Gmelin, P. Rödhammer. *J. Phys. E: Sci. Instrum.* **14**, 223 (1981).
8. M. Sorai, K. Kaji, Y. Kaneko. *J. Chem. Therm.* **24**, 167 (1992).
9. Z.-C. Tan, Q. Shi, B.-P. Liu, H.-T. Zhang. *J. Therm. Anal. Calorim.* **92**, 367 (2008).
10. B. Wunderlich, M. Dole. *J. Polym. Sci.* **32**, 125 (1958).
11. See, for example: Z. Q. Wu, V. L. Dann, S. Z. D. Cheng, B. Wunderlich. *J. Therm. Anal.* **34**, 105 (1988).
12. M. Pyda, E. Nowak-Pyda, J. Heeg, H. Huth, A. A. Minakov, M. L. Di Lorenzo, C. Schick, B. Wunderlich. *J. Polym. Sci., Part B: Polym. Phys.* **44**, 1364 (2006).
13. N. S. Kurnakov. *Z. Anorg. Chem.* **42**, 184 (1904).
14. B. Wunderlich, W. H. Kashdan. *J. Polym. Sci.* **50**, 71 (1961).
15. E. S. Watson, M. J. O'Neill, J. Justin, N. Brenner. *Anal. Chem.* **36**, 1233 (1964).
16. B. Wunderlich, U. Gaur. "Differential scanning calorimetry of flexible, linear macromolecules", in *Polymer Characterization*, C. D. Craver (Ed.), ACS Advances in Chemistry Series, No. 203, pp. 195–208, American Chemical Society, Washington, DC (1983).
17. R. L. Danley. *Thermochim. Acta* **395**, 201 (2005).
18. G. W. H. Höhne, W. F. Hemminger, H.-J. Flammersheim. *Differential Scanning Calorimetry,* Springer, Berlin (2003).
19. M. Reading, D. J. Hourston (Eds.). *Modulated Temperature Differential Scanning Calorimetry*, Springer, Dordrecht (2006).
20. A. Boller, Y. Jin, B. Wunderlich. *J. Therm. Analysis* **42**, 307 (1994).
21. B. Wunderlich, Y. Jin, A. Boller. *Thermochim. Acta* **238**, 277 (1994).
22. B. Wunderlich, A. Boller, I. Okazaki, S. Kreitmeier. *Thermochim. Acta* **282/283**, 143 (1996).

23. R. Androsch, I. Moon, S. Kreitmeier, B. Wunderlich. *Thermochim. Acta* **357/358**, 267 (2000).
24. R. Androsch, B. Wunderlich. *Thermochim. Acta* **333**, 27 (1999).
25. Y. K. Kwon, R. Androsch, M. Pyda, B. Wunderlich. *Thermochim. Acta* **367/368**, 203 (2001).
26. M. Pyda, Y. K. Kwon, B. Wunderlich. *Thermochim. Acta* **367/368**, 217 (2001).
27. J. Pak, B. Wunderlich. *Thermochim. Acta* **367/368**, 229 (2001).
28. A. Toda, T. Arita, C. Tomita, M. Hikosaka. *Polym. J.* **31**, 790 (1999).
29. A. Toda, C. Tomita, M. Hikosaka. *J. Therm. Anal.* **54**, 623 (1998).
30. A. Einstein. *Ann. Phys.* **22**, 800 (1907); correction on p. 800.
31. (a) P. Debye. *Ann. Phys.* **39**, 789 (1911); (b) Tables of Debye functions are available in: J. A. Beattie. *J. Math. Phys. (MIT)* **6**, 1 (1926/27) for three dimensions; (c) U. Gaur, G. Pultz, H. Wiedemeier, B. Wunderlich. *J. Therm. Anal.* **21**, 309 (1981) for two dimensions; and (d) B. Wunderlich. *J. Chem. Phys.* **37**, 1207 (1962); (e) For initial computer programs and discussions, see: Yu. Y. Cheban, S. F. Lau, B. Wunderlich. *Colloid Polym. Sci.* **260**, 9 (1982).
32. E. Schrödinger. In *Handbuch der Physik,* H. Geiger, K. Scheel (Eds.), **10**, 275 (1926).
33. (a) V. V. Tarasov. *Zh. Fiz. Khim.* **24**, 111 (1950); (b) V. V. Tarasov. *Zh. Fiz. Khim.* **27**, 1430 (1953); (c) V. V. Tarasov. *Zh. Fiz. Khim.* **39**, 2077 (1965).
34. J. Barnes, B. Fanconi. *J. Phys. Chem. Ref. Data* **7**, 1309 (1978).
35. B. Wunderlich. *J. Chem. Phys.* **37**, 1207 (1962).
36. (a) J. Grebowicz, B. Wunderlich. *J. Therm. Anal.* **30**, 229 (1985); (b) R. Pan, M. Varma, B. Wunderlich. *J. Therm. Anal.* **35**, 955 (1989).
37. (a) U. Gaur, H.-C. Shu, A. Mehta, B. Wunderlich. *J. Phys. Chem. Ref. Data* **10**, 89 (1981); (b) U. Gaur, B. Wunderlich. *J. Phys. Chem. Ref. Data* **10**, 119 (1981); (c) U. Gaur, B. Wunderlich. *J. Phys. Chem. Ref. Data* **10**, 1001 (1981); (d) U. Gaur, B. Wunderlich. *J. Phys. Chem. Ref. Data* **10**, 1051 (1981); (e) U. Gaur, B. Wunderlich. *J. Phys. Chem. Ref. Data* **11**, 313 (1982); (f) U. Gaur, S.-F. Lau, B. B. Wunderlich, B. Wunderlich. *J. Phys. Chem. Ref. Data* **11**, 1065 (1982); (g) U. Gaur, B. B. Wunderlich, B. Wunderlich. *J. Phys. Chem. Ref. Data* **12**, 29 (1983); (h) U. Gaur, S.-F. Lau, B. B. Wunderlich, B. Wunderlich. *J. Phys. Chem. Ref. Data* **12**, 65 (1983); (i) U. Gaur, S.-F. Lau, B. Wunderlich. *J. Phys. Chem. Ref. Data* **12**, 91 (1983); (j) M. Varma-Nair, B. Wunderlich. *J. Phys. Chem. Ref. Data* **20**, 349 (1991); an online version is available through <http://athas.prz.rzeszow.pl>.
38. (a) U. Gaur, B. Wunderlich. "Advanced thermal analysis system (ATHAS)-polymer heat capacity data bank", in *Computer Applications in Applied Polymer Science*, T. Provder (Ed.), ACS Symposium Series No. 197, p. 355, American Chemical Society, Washington, DC (1983); (b) see also: B. Wunderlich. *Pure Appl. Chem.* **67**, 1019 (1995) and [1].
39. B. G. Sumpter, D. W. Noid, G. L. Liang, B. Wunderlich. *Adv. Polym. Sci.* **116**, 27 (1994).
40. (a) B. Wunderlich. *J. Chem. Phys.* **37**, 2429 (1962); (b) B. Wunderlich. *J. Polymer Sci., Part C* **1**, 41 (1963).
41. Y. Kim, H. L. Strauss, R. G. Snyder. *J. Phys. Chem.* **93**, 7520 (1989).
42. G. Herzberg. *Infrared and Raman Spectra of Polyatomic Molecules*, Van Nostrand, New York (1945).
43. (a) H. Eyring. *J. Chem. Phys.* **4**, 283 (1936); see also (b) N. Hirai, H. Eyring. *J. Appl. Phys.* **29**, 810 (1958).
44. B. Wunderlich. *Thermochim. Acta* **300**, 43 (1997).
45. P. Ehrenfest. *Proc. Acad. Sci., Amsterdam* **36**, 153 (1933).
46. B. Wunderlich, D. M. Bodily, M. H. Kaplan. *J. Appl. Phys.* **35**, 95 (1964).
47. W. Kauzmann. *Chem. Rev.* **43**, 219 (1948).
48. M. Pyda, B. Wunderlich. *J. Polym. Sci., Part B: Polym. Phys.* **40**, 1245 (2002).
49. I. Okazaki, B. Wunderlich. *J. Polym. Sci., Part B: Polym. Phys.* **34**, 2941 (1996).
50. B. Wunderlich, A. Boller, I. Okazaki, S. Kreitmeier. *J. Therm. Anal.* **47**, 1013 (1996).
51. B. Wunderlich, I. Okazaki. *J. Therm. Anal.* **49**, 57 (1997).

52. L. C. Thomas, A. Boller, I. Okazaki, B. Wunderlich. *Thermochim. Acta* **291**, 85 (1997).
53. J. Pak, M. Pyda, B. Wunderlich. *Macromolecules* **36**, 495 (2003).
54. B. Wunderlich. *Progr. Polym. Sci.* **28**, 383 (2003).
55. K. Ishikiriyama, A. Boller, B. Wunderlich. *J. Therm. Anal.* **50**, 547 (1997).
56. K. Ishikiriyama, B. Wunderlich. *Macromolecules* **30**, 4126 (1997).
57. W. Qiu, B. Wunderlich. *Thermochim. Acta* **448**, 136 (2006).
58. W. Qiu, M. Pyda, E. Nowak-Pyda, A. Habenschuss, B. Wunderlich. *J. Polym. Sci., Part B: Polym. Phys.* **45**, 475 (2007).
59. W. Qiu, A. Habenschuss, B. Wunderlich. *Polymer* **48**, 1641 (2007).
60. B. Wunderlich. *J. Therm. Anal. Calorim.* **93**, 7 (2008).